CORONAL EMISSION LINE PROFILE OBSERVATIONS AT TOTAL SOLAR ECLIPSES

I: *Airborne Instrumentation and Results**

D. H. LIEBENBERG
LASL, University of California, Los Alamos, N.M. 87545, U.S.A.

(Received 7 July, 1975)

Abstract. A 25-cm aperture $f/8.0$ telescope was operated aboard a U.S. Air Force – Energy Research and Development Administration aircraft at the 30 May 1965 and 12 November 1966 total solar eclipses. A fixed path Fabry-Perot interferometer spectrograph with 0.008-nm resolution was developed to photographically record intensity vs wavelength profiles of the coronal emission lines Fe XIV (530.3 nm), Fe X (637.4 nm) and Ca XV (569.4 nm). A pressure scanned Fabry-Perot interferometer was developed with a photoelectric detector and recorder. Photoelectric tracking was used in 1965 and gyroscopic tracking with photoelectric updating provided improved tracking in 1966. Photographic interferometer data were obtained out to 1.79 $R_\odot$ in 1965 at 530.3 nm. Doppler shifts are determined and indicate generally small velocities of coronal material. Results in Fe XIV and Fe X were obtained in 1966. No Ca XV emission was detected in 1966.

1. Introduction

Observations of the intensity vs wavelength profile of coronal emission lines provide information regarding the total number of emitting ions and their velocity distribution. The velocity distribution may be related to a kinetic temperature under hydrostatic conditions, or may be used to determine turbulent and flow velocities dependent on the profile shape, as discussed by Krall and Trivelpiece (1973). Such determinations are important in discussions of the heating mechanisms in the corona, such as by Billings (1966). Coronagraphic observations of the emission line profiles are restricted to very near the base of the solar corona. Yet calculations, by Kuperus (1972), of the coronal heating mechanism and the onset of the solar wind show the dependence on the temperature gradient farther out in the corona. The line profiles may be modified by departures from thermal equilibrium and periodic wave excitation, as indicated by Liebenberg and Hoffman (1974). Few systematic studies of these effects have been made although Billings (1966) has considered harmonic oscillations in computed profiles.

During a total solar eclipse the scattered light intensity near the Sun is reduced by about three orders of magnitude which makes possible observations of the emission corona to more than 2 $R_\odot$. An additional advantage for emission line profile measurements is the freedom from the Fraunhofer absorption line that distorts profiles of Fe XIV at 530.3 nm obtained with a coronagraph and that would remain a problem near the limb for spacecraft coronagraphs. The present apparatus was designed to obtain accurate intensity measurements with a high resolution spectrograph and obtain coronal emission line profiles throughout the solar corona at times of solar eclipse.

* Work performed under the auspices of the U.S. Energy Research and Development Administration.

Solar Physics **44** (1975) 331–344.

The apparatus was designed to operate from an aircraft platform: to obtain a further reduction by a factor of two of the scattered sky light intensity, to increase the likelihood of success due to freedom from cloud cover, and to improve the reliability of the logistical support for the equipment. Methods of accurate telescope pointing were developed to maintain tracking control of the corona for times long compared with photographic exposure times. The apparatus has been modified for each eclipse to adapt observations to the available time of totality and to the particular solar altitude. The aircraft, a modified NC-135 military version of the Boeing 707, was operated for the U.S. Energy Research and Development Administration by the U.S. Air Force. This paper will describe the instrumentation at the total solar eclipses of 30 May 1965 and 12 November 1966. Results of these observations are discussed in the following paper and by Liebenberg *et al.* (1975) (referred to as LBW).

2. Instrumentation

We required a large aperture telescope limited by the aircraft window size, with focal length permitting better than 3″ resolution on relatively fast photographic emulsion, and a compact spectrograph for the accurate analysis of emission line profiles; these instruments to be accurately tracked to the solar corona when mounted in the NC-135 aircraft. An effective focal ratio of $f/8$ was chosen to provide exposure times of 30 s for expected emission line intensities of Fe XIV (530.3 nm) at 1.5 $R_\odot$. The lens design by Brixner (1966) has been previously described. A refracting telescope was designed since tracking over a large angle, ± 5 deg, of the 25-cm aperture telescope through a nominal 30 cm square window required the objective to be gimballed near the window. Further, the large field of view required, 2.5°, suggested a refractor as the objective element. The lens, an oil cemented doublet with a wide field, has an aperture of 25 cm and a focal length of 202.1 cm.

At the 1965 eclipse, the altitude of the Sun was about 50° and a side window of aperture 30 cm × 30 cm was used. An optical quality window, 1.9 cm thick, was installed to reduce strain birefringence and possible effects on the profile of the 530.3-nm line, shown by Hyder *et al.* (1968) to be partially polarized. At mid-totality the bearing of the aircraft was selected to provide a backward look angle of 4°, thus minimizing window reflections within the instrumentation.

The instrumentation behind the objective lens was different at the 1965 and 1966 eclipses. At the 1965 eclipse, a table provided the telescope mount and components were set on the optical bench that was fixed ridgidly to the aircraft, as shown in Figure 1. Two-axis guiding was possible with the tracking mirror. Behind the objective lens a partially reflecting mirror was installed at 45° to the optic axis. Approximately 8% of the light was reflected to a focus on the photoelectric tracker image plane. A 16-mm pin-registered cine camera was located to photograph the tracker image plane for post eclipse analysis of tracker performance. A sequence of frames from the eclipse is shown in Figure 2. The fiber optics in the tracker focal plane provide good fiducial points for motion analysis.

Coronal light at the main focal plane was divided among three instruments, a photoelectric interferometer, a photoelectric photometer, and a photographic interferometer. Fiber optics set at the primary focus directed light into the first two instruments and the residual light passed into the photographic interferometer. An R, θ holder for the fiber optics permitted the position of the fiber optics to be changed during totality, according to a pre-arranged plan.

The photoelectric interferometer was linked by fiber optics and always operated on axis. The technique has several advantages, such as constant dispersion for various positions in the telescope field of view. A 14.8 cm focal length doublet collimated the beam and it was passed through a predispersing element that was a multilayer dielectric filter (Thin Films, Inc.), the pressure scanned Fabry-Perot interferometer, a matching 14.8 cm focal length doublet, and onto the photo-cathode of a 9558 EMI photomultiplier. The predispersion filter could be selected from those set in a wheel that included the selected emission lines, 530.3 nm (Fe XIV), 637.4 nm (Fe X), 569.4 nm (Ca XV) and 546.1 nm (Hg) for calibration. The aperture was provided by the fiber optics dimension. A single filament 0.025 cm dia fiber was used.

The photoelectric photometer has been described in detail elsewhere by Robertson *et al.* (1965) and was used to obtain integrated line and continuum intensity measurements in selected wavelengths at several locations in the corona during the eclipse.

The photographic interferometer was located on the optic axis of the objective. Residual light from the primary focus was collimated through a 15.2 cm focal length Aero-Ektar (Eastman Kodak) lens. A fixed spacing Fabry-Perot interferometer with a 50 mm aperture followed a predispersing element that was a multi-layer dielectric

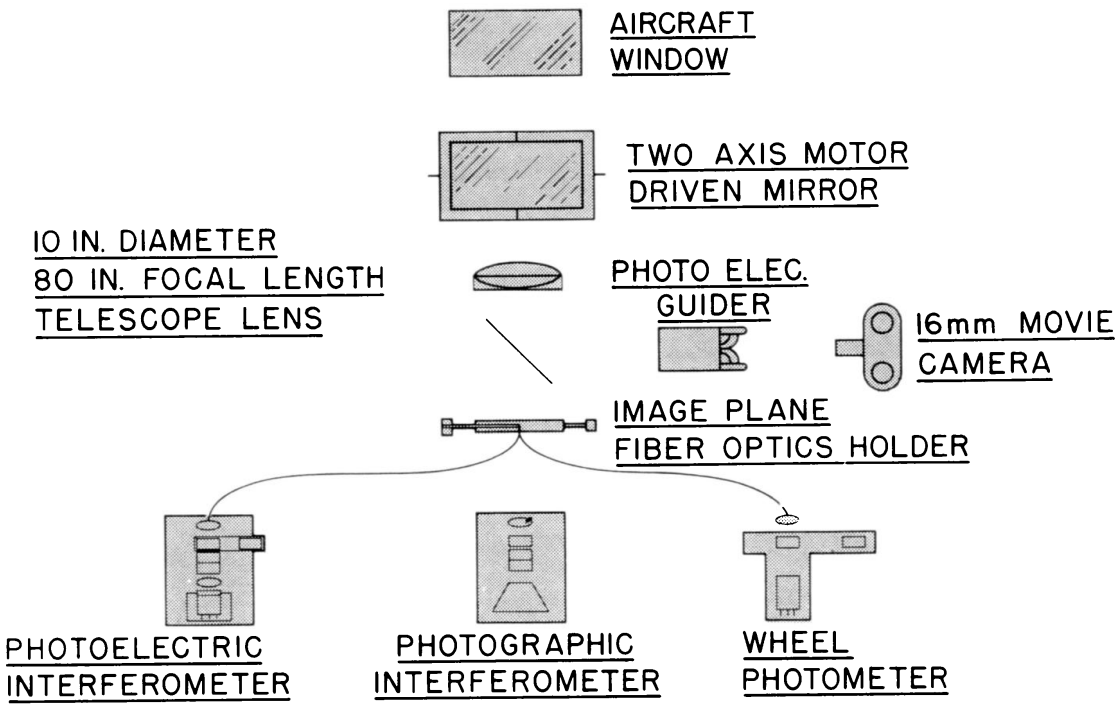

Fig. 1. Schematic optical layout for the 30 May 1965 total solar eclipse. The equipment was mounted on an optical bench installed in the NC-135 aircraft.

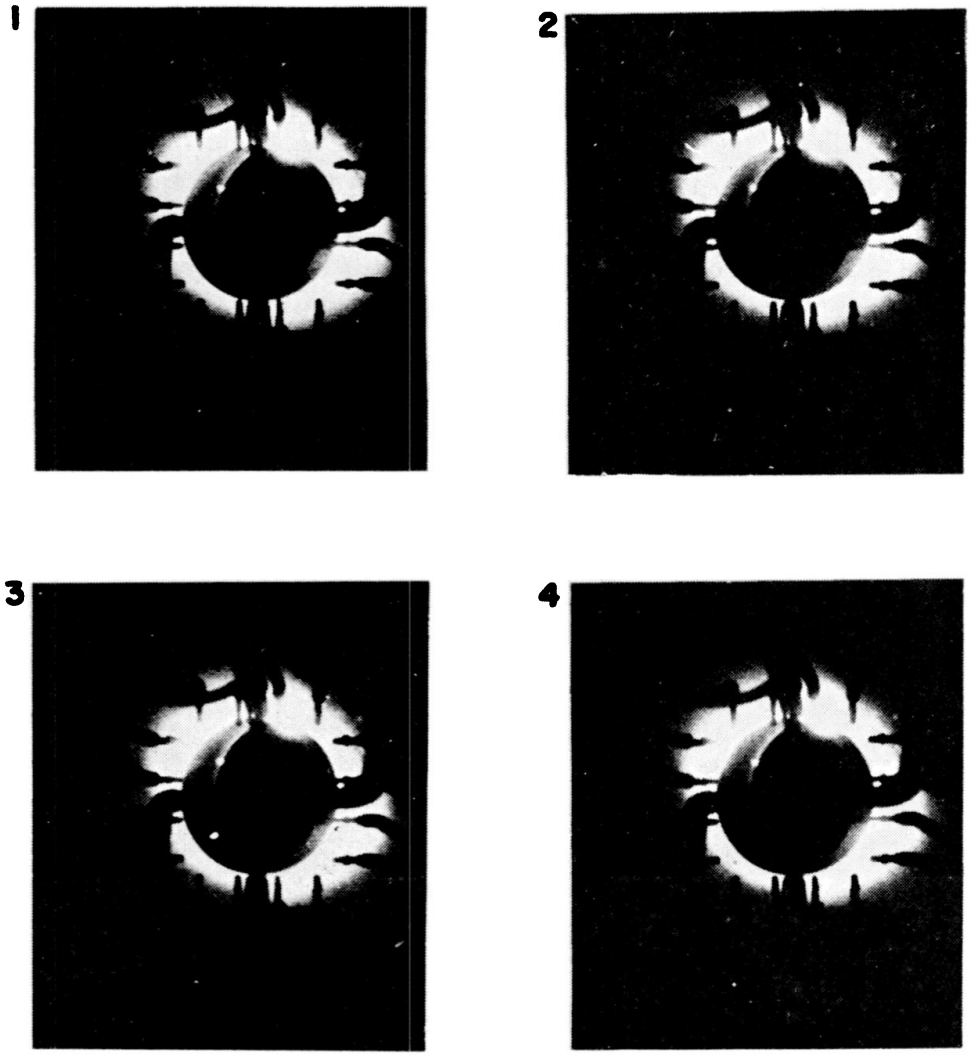

Fig. 2. A sequence of 16-mm cine camera of tracking frames at time intervals of 0.5 s. Rows and columns of fiber optics provide feedback to the photoelectric tracker. A secondary reflection indicates a prominence location. Jupiter is visible on the original print. Slight coronal image motion is detectable between frames 1 and 2 but not between succeeding frames.

interference filter at the wavelength 530.3 nm. A matching lens refocussed the light onto a photographic plate, Kodak type 103aG glass backed.

At the 1966 eclipse, a rigid telescope tube was designed to keep the instruments at the focal plane of the lens within ± 0.002 cm under the expected dynamic forces during moderate inflight turbulence of the aircraft. Three-axis tracking was desired with two-axis motion provided by the double gimbal near the objective lens and the third axis of rotation was available by rotation of the telescope tube. A double set of roller bearings in the telescope tube was used. Measurements of the frequency and amplitude spectrum of the aircraft vibrations and the mass of the telescope were used to set the upper limit of control to 10 Hz for the hydraulic tracking system.

A high altitude solar angle at the 1966 eclipse required the telescope to be mounted below a 40-cm dia window. Along the main optical beam, a partially reflecting plate

was installed at 45° to the optic axis to provide an image on the tracker focal plane, shown in Figure 3. At an opposite aperture, also perpendicular to the axis, a pin-registered 16-mm cine camera was located that photographed both the tracker image and main image plane with nearly equal intensity. In addition to providing tracker operation data up to frequencies of 10 Hz, the camera provided information of the orientation of the coronal image on the dissected focal plane.

Below the partially reflecting plate the third axis tracking bearing permitted the whole telescope to be rotated by 180° and locked into the new tracking position without losing track on the other two axes. In the lower barrel near the primary focus, a fully silvered mirror was mounted to direct about one half the image into the photographic interferometer mounted rigidly to the barrel of the telescope. The other half of the image was formed onto the dissected focal plane, shown in Figure 4. This arrangement permitted nearly full light for each instrument and reduced reciprocity-law

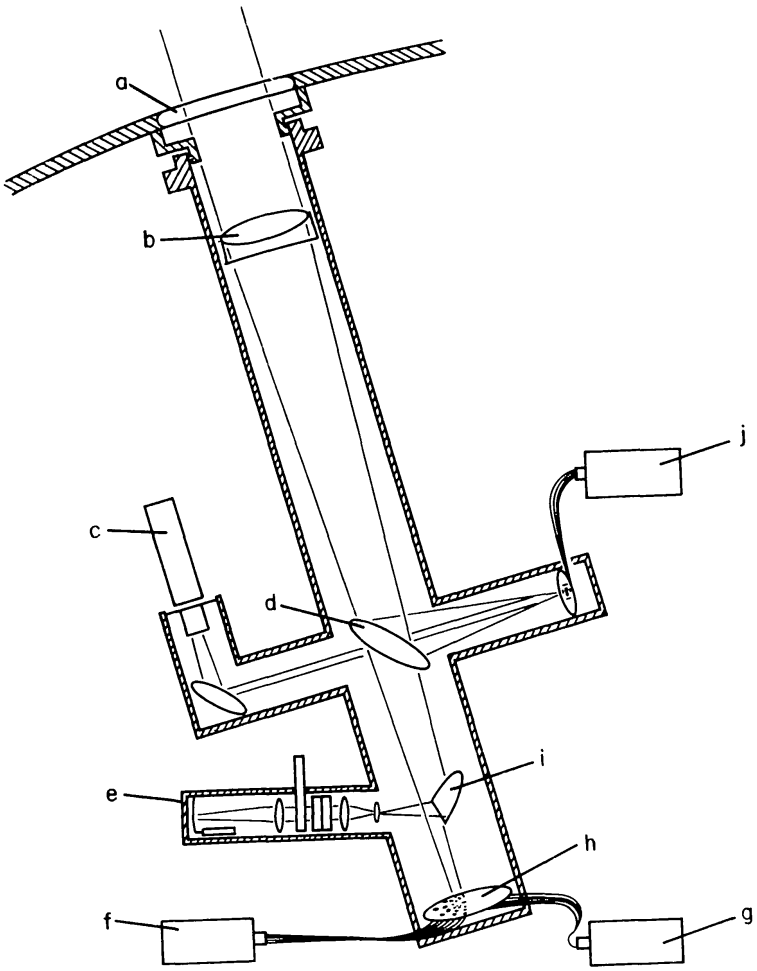

Fig. 3. Schematic optical layout for the 12 November 1966 total solar eclipse. The labeled components are: Aircraft window 38 cm aperture (a), the 25 cm objective doublet (b), a pin-registered 16-mm cine monitor camera (c), the 0.08 reflectance beam splitter (d), the photographic interferometer (e), the photoelectric pressure scanning interferometer (f), the photoelectric photometer (g), the image dissecting focal plane (h), the dividing image mirror (i), and the photoelectric tracker and focal plane (j).

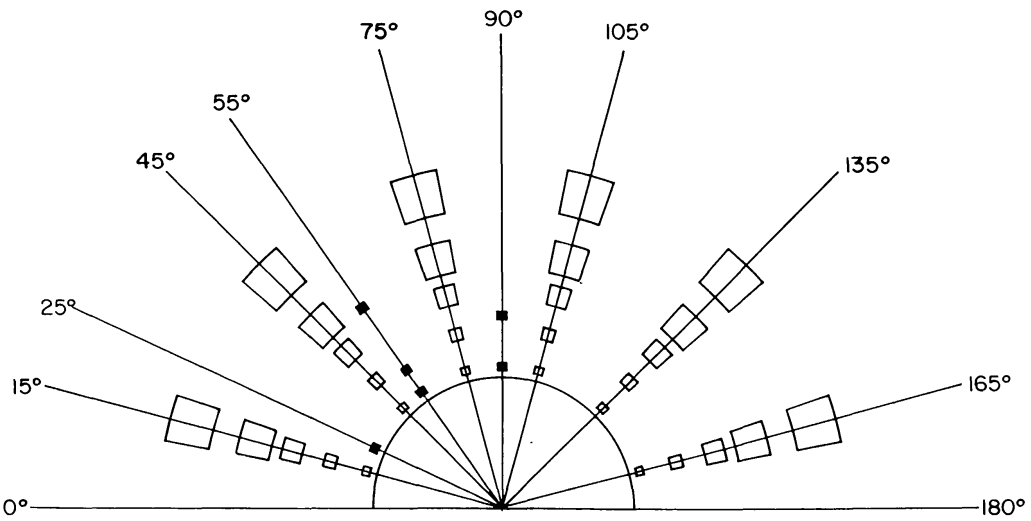

Fig. 4. Image dissected focal plane. Fiber optics with multiple fiber strands sized to equalize the light intensity into the photoelectric photometer are shown as the open squares. Single strand tapered fibers for the photoelectric interferometer are shown as the solid squares. The inner half circle indicates the lunar size at totality and the position angles are relative.

failure of the film and reduced the averaging time for photoelectric measurements. The instrument positions were interchanged mid-way through totality.

The photoelectric photometer was similar to that used in 1965 by Robertson *et al.* (1965), but with an improved design by M. Robertson, having in the focal plane a set of 30 fiber optics the diameter of which was a function of position in the image plane. Although the fibers were fixed in the focal plane plate this plate could be separately rotated by $\pm 15°$. This rotation of the focal plane provided an opportunity for the operator to line up a set of fibers on a predicted or observed streamer or active coronal region during totality.

The photoelectric interferometer was similar to that used in 1965. An improved amplifier was developed and an RCA 7265 photomultiplier tube was used. Pressure scanning was accomplished by mounting the complete interferometer into a separate cell with anti-reflection coated windows that could be pressurized to 4.14 bar and automatically cycled. In practice, scans of one and one half interferometer orders were used by adjusting the maximum pressure of the system.

Solenoid valves controlled gas flow into and from the pressure cell, the gas pressure upstream was maintained at more than one atmosphere above the maximum pressure. A sensor permitted measurements to 0.19% accuracy and these data were recorded on analog magnetic tape. The accuracy was adequate to assure that the measured profiles were linear in wavelength. This was verified before and after totality from measured scans of the mercury light source at 546.1 nm. Freon 12 gas was used as the pressurant and the cell was designed to have very low volume so that scan rates of 1 order per 2 s were readily obtained. This scan rate conveniently matched the interferometer resolution and the amplifier response. Six fiber optics could be presented in the object focal plane on axis of the interferometer. A stepping motor and detents placed these fibers to an accuracy of better than 0.03 mm in the focal plane. An operator could

select the fiber and thus the coronal region desired from the control panel. The fiber optics were especially designed for this instrument. The entrance aperture at the focal plane of the primary image was 0.76 mm diam, while the exit aperture to the interferometer from the tapered fiber was 0.25 mm. The design permitted improved wavelength resolution in the interferometer without the light loss that would result by introducing an aperture in front of the photomultiplier. The $f/3$ optics of the interferometer matched reasonably well the large solid angle of the fiber optic exit beam.

The photographic interferometer was modified from that used in 1965. Since only half the field of view was available at one time from the turning mirror, a 70-mm adapted Hasselblad camera back was used so that film could be advanced more quickly than by changing glass plates. Kodak type 103G film was used on an Estar™ base film. There was some loss of sensitivity due to the thinner emulsion on the film base. Finally, the filter wheel containing a sequence of pre-dispersing filters was automated, thus, an operator could remotely select the filter and exposure time and operate the electric film advance. The instrument could be bolted into place on the telescope or taken off for alignment, without disturbing the focus and alignment with the primary image.

Selection of the dielectric interference filter characteristics required compromise between the desire to eliminate continuum coronal light and thus enhance the signal-to-noise ratio, and the necessity to keep the filter transmission from influencing the shapes of the emission line profile. These requirements were met with a filter having a full width at half maximum intensity points of 1.2 nm. The variation of intensity over the 0.4 nm wavelength region centered at maximum transmission was only a few percent and good signal-to-noise or line-to-continuum ratios were obtained out to 1.8 $R_\odot$. Blocking of the filters over the wavelength range beyond this selected wavelength, but within the instrumental sensitivity, was provided by additional filters. Spectrographic determinations of the center wavelength, pass bandwidth, and blocking characteristics were made for each filter at the specified temperature of 25 °C. A constant temperature control to 25 °C of the filter was provided in the instruments.

The interferometer plates were specified to be flat to 1/100 wave at 546.1 nm. Spacers for the plates were made from sapphire watch jewels and were of the point plane type. The spacers were made to the same thickness within the accuracy 0.003 mm. Further adjustments to obtain parallelism of the interferometer plates were achieved by lapping and finally with spring pressure in the interferometer cell. This resulted in small plate distortion which did not change the measured finesse of the interferometer. The dielectric coatings on the plates increased the reflectivity to 0.97 and the finesse was probably limited by the non-uniformities in the plate surfaces, as discussed by Chaball (1953). Without considering plate flatness the reflectance R gives a finesse of

$$F = \pi \left[\frac{R}{(1-R)^2} \right]^{1/2} . \tag{1}$$

In the present case $F = 103$.

The slight spring pressure also served to stabilize the plates against aircraft environment. The interferometer plates were spaced 0.382 mm apart to give a free spectral range of 0.368 nm. A resolution of 0.008 nm at 530.3 nm was determined from measurements of Hg profile. This spectral resolution compared favorably with the small Climax coronagraph where the instrumental width at 530.3 nm has been reported by Billings (1966) to be 0.015 nm. The plate scale dispersion in first order for the interferometer was 10 Mm m^{-1} (1 mm $Å^{-1}$) an optimum value as discussed by Billings (1966).

Tracking the eclipsed Sun with a photo-electric system cannot be completely described within the limitations of this paper. The general method is given and the results are discussed with direct bearing on measured line profiles. At the 1965 eclipse, the tracker was completely photoelectrically controlled. Manual control brought the solar image into view to roughly center the image on the tracker plane light fibers optically linking the photomultiplier detectors. The feedback loop around these detectors and the mirror servo motors were used to maintain automatic tracking control. This system worked very well, in part because the eclipsed Sun has a steep gradient in light, both out into the solar corona where $I \sim R^{-6}$ approximately, and into the lunar disk where scattered light in the optical system and Earth shine make up the two contributions to a measured intensity. In the tracker focal plane, shown in Figure 2, the fibers that sense the gradient of light were bisected by the correctly centered image. Also shown, are the several fibers used to supply feedback to bring about a recovery of the system following a loss of track by the fine control. The bandwidth of the fine control was about 7 Hz. As the frame sequence indicates and the full movies show in detail this system more than met the design criteria. At the 1965 eclipse, the recorded output of the photoelectric sensors indicated an overall RMS tracking error of 0.7′ or 42″.

At the 1966 eclipse, several modifications were developed in the tracking system to accommodate the tracking of the telescope tube to which other instruments were optically or mechanically attached. While photoelectric sensors provided the error signal for the fine tracking control in the two gimballed axes, a gyro control was added to provide a backup and to permit fast recovery and initial acquisition through the partial phases of the eclipse. A gyro controlled servo motor drive with a constant offset rate was used for control of the rotation axis. Manual guidance in a rate control mode with a control stick was an alternative to the automatic modes that could be independently selected for each axis. A battery operated control directly connected to the hydraulic servo valves was a safety feature in connection with the hydraulic high pressure accumulator. The performance of the tracker during totality as monitored by the cine camera was found to be $\pm 15''$. Additional sensors to monitor the hydraulic rod position and photoelectric tracker error signal were installed and their outputs recorded during flight. These data agreed with the cine camera value of tracking error during the full totality time.

3. Operation

The general operations of the flight and the instrumentation have been reported by

Cox *et al.* (1965) and Cox *et al.* (1967). At the 1965 eclipse, an altitude of 12.25 km was maintained during the $4^m\ 47^s$ of totality. The photographic interferometer was operated to obtain a sequence of plates with exposure times varying from 1 to 30 s as listed in Table I. Plates were changed manually during totality so that a total of eight images on four plates was obtained. Additional plates were carried along to have the same thermal history and were later exposed with more accurate step wedges. A step wedge calibration was applied to each eclipse plate, although the quality of this wedge was poor. Development was 8 m in Kodak D-19 at 68 °F. Exposure times of 10 s and longer provided good images of green line emission profiles from the coronal features on the west limb. Calibration was carried out for both the wavelength and intensity. A mercury source was shined through the complete optical system to give instrumental profiles in addition to information about the vignetting of the system at full aperture. An opal glass filter with nearly 13-cm aperture was used to calibrate measured intensities to the full Sun and was calibrated by Newkirk (1965). The radiance at 554.0 nm was determined to be 8.3×10^{-7}. In addition, the solar absorption line spectrum gave a good calibration of the pass band of the interferometer and the predispersion filter. Since the opal glass was not as large as the full telescope aperture, additional exposures were obtained using Kodak gelatin neutral density filters across the full aperture. Exposures were obtained at practice flights of the full Moon to check both the focus of the system and to provide an alternative intensity standard. In practice the most reliable intensity calibration was provided by the laboratory maintained xenon flash lamp and step wedge. As will be shown in the following paper, the minimum integrated intensity of Fe XIV emission for which an accurate line profile was obtained was 0.13 millionths of the solar disk intensity. This sensitivity compares favorably with more recent instrumentation. The successful operation of the photoelectric photometer has been reported by Robertson *et al.* (1965) and the photoelectric interferometer provided no output at this eclipse.

The 1966 eclipse was observed at an altitude of 9.94 km and had a duration of $2^m\ 40^s$. The photographic interferometer was operated to obtain a sequence of 20 s and10 s exposures at the wavelengths, 530.3, 569.4, 637.4 nm and calibration procedures were similar to those in 1965. The wedge calibrations were placed on a separate spool of film which was all cut from the same lot and had the same thermal history as the eclipse film. Development was simultaneous with the eclipse films.

TABLE I

Exposure time and plate sequence where the UT of each exposure mid point is given in min after 20^h

Plate No.	Exposure time	Mid point time
1	10 s, 30 s	13^m26^s, 13^m45^s
2	1 s, 10 s	14^m23^s, 14^m41^s
3	30 s, 1 s	15^m20^s, 15^m46^s
4	30 s, 10 s	16^m19^s, 16^m54^s

The photoelectric interferometer was operated with the new amplifier, although the sensitivity of the instrument, due partly to the light loss through the fiber optics and the fainter corona, was not as great as desired. Instrumental profiles obtained with the mercury source lamp also calibrated the interferometer order scan rate on the recorded output. The operator selected the predispersion filter 530.3 nm, 637.4 nm, or 546.1 nm Hg by actuating a filter wheel and could activate the stepping motor to bring a different fiber to the optic axis of the pressure scanned interferometer. The signal to noise ratio of the resultant data was not large.

4. Results

At the 1965 eclipse, the series of images gave good line profile information in regions above the west limb, including the coronal condensation at $\phi = 295°$ heliographic position angle, the helmet streamer at $\phi = 320°$ and in the quiet region $\phi = 255$–$280°$. An isodensity trace of the 10-s exposure on Plate No. 2 is shown in Figure 5. Heliocentric coordinates were determined from the apparent position of Jupiter, clearly seen on each frame of the cine camera, where the position angle of Jupiter was known to be $\phi = 223.7°$ for the time and location of totality. The center of the fringe defines a coordinate system that was useful for measurement of the fringe, since it was important that the slit of the microdensitometer was driven along a radius vector in this system. To check the center position that is indicated on Figure 5, the fringe radius R is calculated from the equation

$$R^2 = \frac{n_1 f^2 \lambda_0}{n_2^2 d} (p - 1 + e), \tag{2}$$

where f is the focal length of the final lens at the wavelength of the line λ_0, the plate separation is d and the order of the fringe is p. The fractional order is e and the indices of refraction external to the plates, n_2, and internal to the plates, n_1, were assumed to be 1.0. Equation (2) is solved with measured data from the first two fringes and subsequent calculations for the successive fringes are shown in Table II.

TABLE II

Calculated and measured positions of the fringe system on Plate No. 2, 10 s exposure. Fringes numbered 2 and 3 were used to solve Equation (2)

Fringe	Measured	Calculated
2	(0.503 cm)	(0.503 cm)
3	(0.738)	(0.738)
4	0.919	0.919
5	1.068	1.068
6	1.200	1.199
7	1.318	1.317
8	1.432	1.425

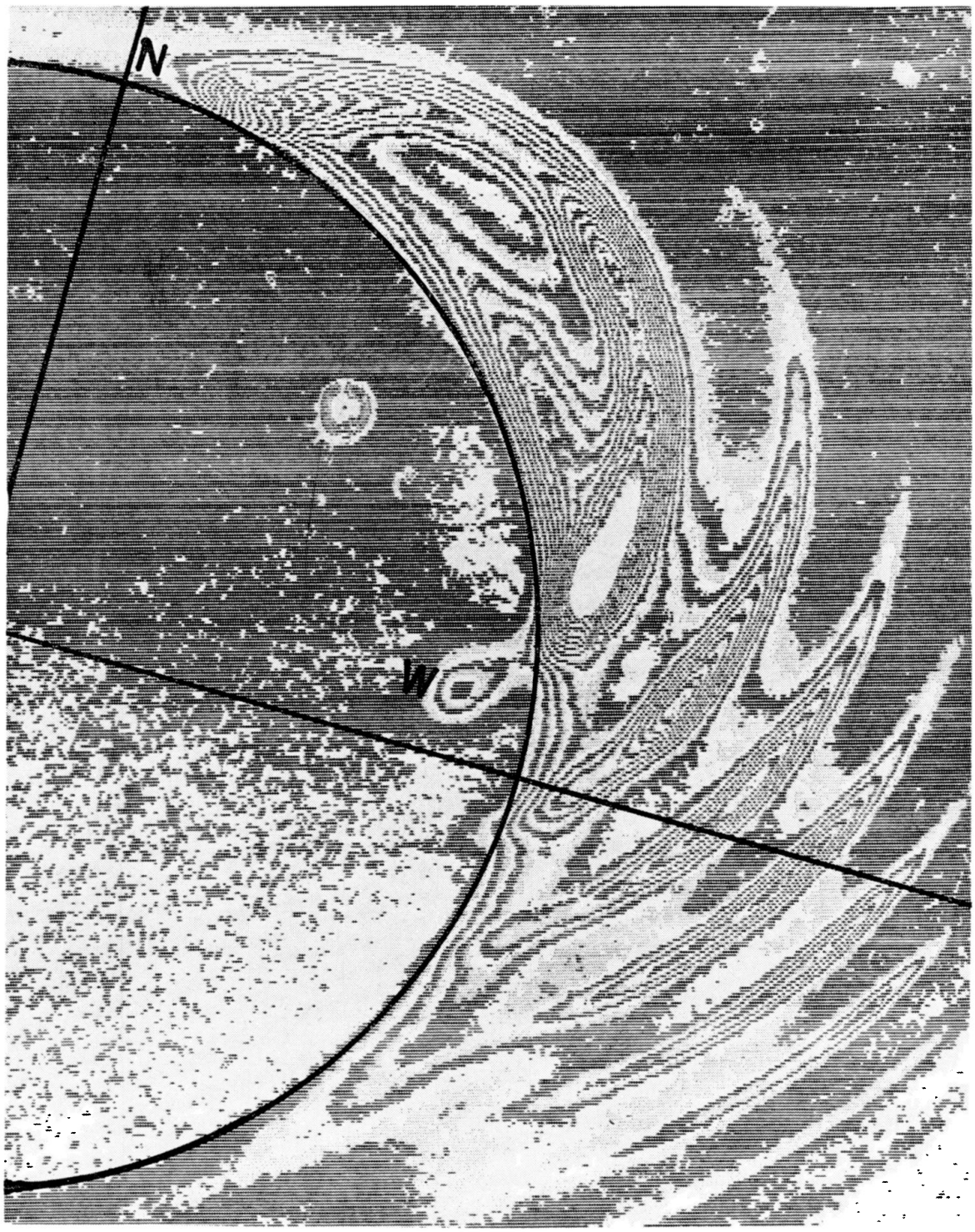

Fig. 5. Isodensity tracing of the photographic interferometer image obtained at the 1965 total solar eclipse. The heliocentric coordinates have been overlaid and the lunar limb position indicated.

The solar and lunar image sizes were determined to be within 0.25 mm of those calculated from the measured focal length of the objective and the assumption of equal focal lengths for the matched interferometer lenses.

Doppler shifts of the lines are obtained from departures of the measured fringe diameters from those in Table II. The limit of resolution is ~ 0.03 mm or ~ 4 km s^{-1} depending on the fringe order. To this limit of resolution no Doppler velocities are detected in fringes 5 through 8. The Doppler shifts in fringe 2 were discussed by LBW. There is a region at $\phi = 277°$ where the Doppler velocity $v_0 = +2$ km s^{-1} (toward the observer) is detected in fringe 4 and a region from $\phi = 267$–$285°$ where Doppler velocities are measured. At $\phi = 284°$ in fringe 3 $v_0 = +7$ km s^{-1}. In the outer fringe a Doppler velocity $v_0 = -2$ km s^{-1} is detected at $\phi = 284°$.

These data indicate that the coronal material has only very small Doppler velocities in this region, in marked contrast to the results of Delone and Makarova (1969) who list velocities in this region up to 149 km s^{-1} and indicate a much greater irregularity in motions than are indicated from the present data.

An initial set of tracings with a 50 $-\mu$m square slit of the microdensitometer were obtained. A typical tracing is shown in Figure 6, redrawn from the original to preserve the actual noise. This tracing is at a 50° angle in the fringe coordinate system and is selected to show the signal-to-noise ratio out to fringe number 8 at 1.79 $R_\odot$. This is the farthest radial distance from the center of the disk that useable profiles were recorded.

In addition to the line profile there is a background intensity that is continuum emission passed by the predispersion filter. This K+F corona component will be discussed as part of the data reduction in the following paper.

The 1966 data from the photographic interferometer include Fe XIV and Fe X emission line profiles. These data are not so extensive due to reduction of sensitivity with the film base. In addition, a photograph was taken at the Ca XV emission line at the wavelength 569.4 nm and no Ca XV emission was detected. This agrees with

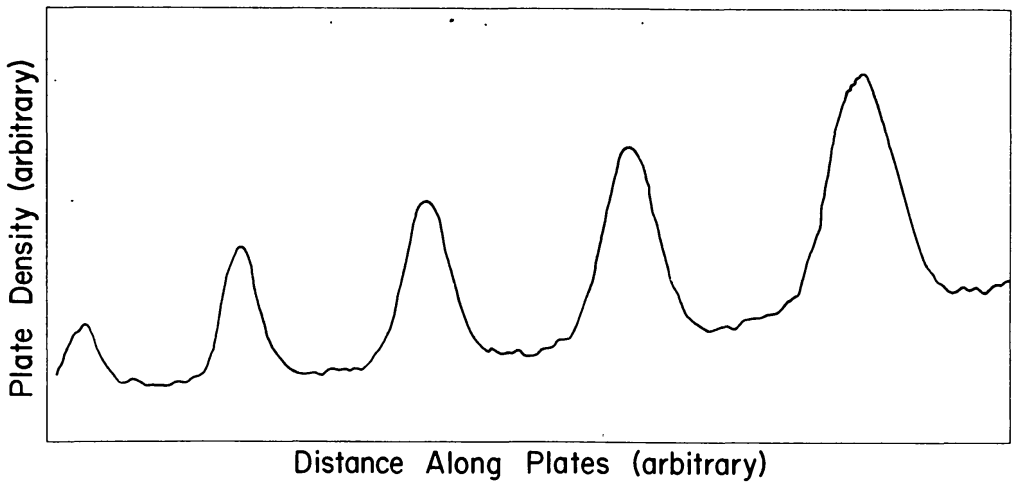

Fig. 6. Microdensitometer tracing of the Plate No. 2 10 s exposure as redrawn. The square slit corresponds to 5″ in the sky.

coronographic measurements. An interesting visual observation that supports the conclusions that the instrument has low scattered light was the observation of the white light corona for 90 s after 3rd contact on the opposite limb of the Sun.

Successful operation obtained with the photoelectric pressure scanning interferometer and with the filter photometer.

5. Conclusion

The instrumentation described here was successfully operated at the 30 May 1965 and 12 November 1966 total solar eclipses. Measurements were obtained of the coronal emission line intensities, full width at half maximum intensity points, profile shapes, and Doppler shifts of the line center. Some discussion of these coronal observations was given by LBW. Further results are reported in the following paper. This instrumentation has been further developed with a video recording system that has been used at recent eclipses, as described by Hoffman *et al.* (1975), and inflight tracking to $\pm 5''$ was achieved at the 30 June 1973 eclipse.

Acknowledgements

The instrumentation development was significantly aided by several members of the Los Alamos Scientific Laboratory staff. It is my pleasant duty to thank Mr Ed. Brown, Mr J. Calligan III, Dr A. Cox, Mr James Hill, Dr Marvin Hoffman, the late Robert Lang, Dr William Ogle, Dr Ralph Partridge, and Dr Joseph Perry who, among others, contributed significantly to this project. The Sandia photometer and, in 1966, the fabrication of the fiber optics focal plane at the Sandia Corporation were directed by Dr Merton Robertson.

Members of the observing team, not already acknowledged above, included Mr L. Black, Dr K. D. Williamson, Mr W. Wolff, and members of the U.S. Air Force, in particular Col. N. Garland and Col. J. Wells, provided essential support for the successfully obtained observations. We are grateful to Dr Gordon Newkirk, High Altitude Observatory of the National Center for Atmospheric Research, for providing the calibrated opal glass filters.

References

Billings, D. E.: 1966, *A Guide to the Solar Corona*, Academic Press, New York.
Brixner, B.: 1966, *Appl. Opt.* **5**, 1207.
Chabball, R.: 1953, J. Res. Center, National Research Sciences Labs., Bellevue (Paris) No. 24, 138.
Cox, A. N., Liebenberg, D. H., and Stone, S. N.: 1965, *Sky Telesc.* **30**, 72.
Cox, A. N., Liebenberg, D. H., Brownlee, R. R., Rudnick, P., and Robertson, M. M.: 1967, *Sky Telesc.* **33**, 85.
Delone, A. B. and Makarova, E. A.: 1969, *Solar Phys.* **9**, 116.
Hoffman, M. M., Sanders, Wm. M., and Liebenberg, D. H.: 1975, *Optical Engineering* **14**, 76.
Hyder, C. L., Mauter, H. A., and Shutt, R. L.: 1968, *Astrophys. J.* **154**, 1039.
Krall, N. A. and Trivelpiece, A. W.: 1973, *Principles of Plasma Physics*, McGraw-Hill, New York.
Kuperus, M.: 1972, in E. Dyer (ed.), *Solar Terrestrial Physics/1970, Part I*, D. Reidel Publ. Co., Dordrecht, Holland, p. 9.

Liebenberg, D. H. and Hoffman, M. M.: 1974, in G. Newkirk (ed.), 'Coronal Disturbances', *IAU Symp.* **57**, 485.
Liebenberg, D. H., Bessey, R. J., and Watson, B.: 1975, *Solar Phys.* **40**, 387.
Liebenberg, D. H., Bessey, R. J., and Watson, B.: 1975, *Solar Phys.*, this issue, p. 345.
Newkirk, G.: 1965, private communication.
Robertson, M. M., Mattison, M. T., and Liebenberg, D. H.: 1965, Sandia Corporation Rept. DC-65-1826, December.